ACS OMEGA

Open Access

http://pubs.acs.org/journal/acsodf

Article

Influence of Controlled Chirality on the Crystallization of Maleimide-Functionalized 3,4-Ethylenedioxythiophene (EDOT-MA) Monomers

Shrirang S. Chhatre, Samadhan S. Nagane, Yuhang Wu, Junghyun Lee, Glenn P. A. Yap, and David C. Martin*

Cite This: *ACS Omega* 2024, 9, 13655−13665

Read Online

ACCESS | Metrics & More | Article Recommendations | Supporting Information

ABSTRACT: Conjugated poly(alkoxythiophenes) such as poly(3,4-ethylenedioxythiophene) (PEDOT) have attracted considerable interest for use in a variety of applications such as biomedical devices, energy storage, and chemical sensing. Functionalized versions of the 3,4-ethylenedioxythiophene (EDOT) monomer make it possible to create polymers with properties tailored for specific applications. The maleimide functional group shows particular promise due to the wide variety of chemical modifications that it can undergo. Here, we examine the role that control of the chirality of the maleimide (MA) substituent has on the crystal structure and crystallization of the EDOT-MA monomer. We describe a method for the synthesis of a homochiral (*S*) variant of EDOT-MA and compare its crystallography, morphology, and thermal properties to that of the (*R*,*S*) EDOT-MA racemic compound. The conformation of the EDOT-MA molecule was substantially different, with the molecules adopting an "L" shape in the homochiral crystal, while in the racemic crystals, they were more colinear. The thermal stability of the homochiral crystals (T_m = 128.6 °C) was slightly higher than the racemic ones (T_m = 102.8 °C). We expect these results to be important in better understanding the solid-state assembly of the corresponding polymers prepared from these monomers.

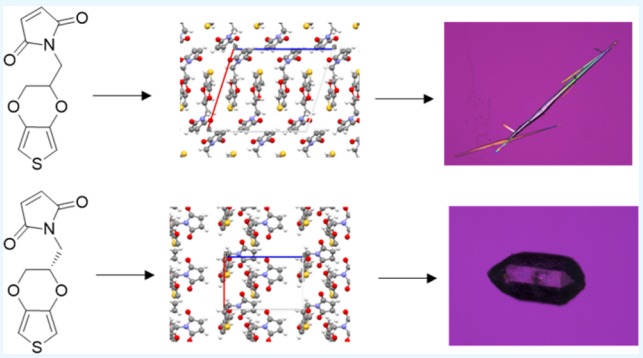

1. INTRODUCTION

Conducting polymers have attracted great interest recently due to their ability to form extended conjugated pathways that facilitate electronic and ionic transport. Being organic in nature, their mechanical and physical properties are significantly different than those of inorganic conducting materials. They have been investigated for use in a variety of applications such as organic electrochemical transistors,[1,2] capacitors,[3,4] photovoltaics,[5,6] electrochromic displays,[7] bioelectronics,[8] and chemical sensors[9]

Poly(3,4-ethylenedioxythiophene) (PEDOT), in particular, has received considerable attention due to its low oxidation potential,[10] high conductivity,[11] low toxicity,[12,13] and high chemical and thermal stability.[14] Due to its ability to conduct both electronically and ionically, PEDOT is an attractive candidate for interfacing ionically conducting living tissue and electronically conducting biomedical devices.[15,16]

A powerful strategy for improving the electrical and biological performance of PEDOT has been to chemically modify the 3,4-ethylenedioxythiophene (EDOT) monomer.[17,18] We have recently synthesized a group of modified EDOT monomers and demonstrated their polymerizability.[19] The maleimide-functionalized monomer 2′-maleimideomethyl -3,4-ethylenedioxythiophene (EDOT-MA) is of particularly high interest because maleimides can react with an array of functional molecules. For example, maleimides readily react with the thiols[20] and amines,[21] which are ubiquitous in biological molecules such as peptides and enzymes.[22] Thus, the presence of the maleimide functionality opens up the possibility of using a host of different biomolecules to improve the biological performance of PEDOT.

In our previous work, we have demonstrated the ability of EDOT-MA to react with proteins containing free thiol groups[23,24] through thiol-maleimide click chemistry. Importantly, we also showcased the ability of EDOT-MA monomers to be modified with a range of biomolecules and amino acids like cholesterol, adamantane, and cysteine. We also demonstrated that these modified monomers retain their ability to be polymerized electrochemically.[25]

We have also demonstrated that polymers made from racemic EDOT-MA (PEDOT-MA) form continuous films that

Received: October 5, 2023
Revised: January 15, 2024
Accepted: January 31, 2024
Published: March 11, 2024

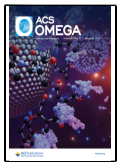

show improved capacitive behavior.[4] The UV absorbance of these polymers is similar to that of unmodified PEDOT, indicating the formation of an extended molecular conjugation. Electrochemical impedance spectroscopy data confirm this with over 3 orders of magnitude drop in the low-frequency region (less than 1 kHz) critical to biological function.

1.1. Importance of Chirality. Due to the nature of biomolecular interactions, it is important for us to understand and control chirality in these molecules. Singly functionalized EDOT monomers have a chiral center at the sp^3 hybridized carbon where the side group is attached onto the alkoxy ring. The previous version of EDOT-MA did not control the stereochemistry of this site and so corresponded to a racemic compound of both *R* and *S* enantiomers.[19]

It is well known that chirality can influence crystal size, shape, and the associated materials properties. Louis Pasteur noted the differences in crystal shape and size for the enantiomers of tartaric acid in 1848,[26] which led to a difference in compressive strength and fracture toughness by 33 and 66%, respectively.[27] In 1886, Arnaldo Piutti discovered that enantiomers of asparagine had different crystal shapes. He also discovered that there was a striking difference in the taste of L-asparagine and D-asparagine, with the former being tasteless and the latter being intensely sweet. This became the first example of chiral selectivity in receptor-mediated biological activity.[28]

In addition to formation of enantiopure crystals, solutions of racemic enantiomers often form crystals with both enantiomers present in the unit cell.[29] These types of enantiomers are called racemic compounds or racemates in the literature as opposed to racemic mixtures, which are composed of equal quantities of enantiopure crystals. The presence of both enantiomeric forms in the unit cell of a racemic compound often leads to different crystal structures and material properties compared to homochiral crystals. Perlovich and co-workers found that racemic compounds and homochiral ibuprofen formed crystals in differing space groups and unit cell dimensions due to hydrogen bonding.[30] These differences in chirality can have profound effects on the chemical properties of drugs. Ibuprofen, along with ketoprofen, and omeprazole are all common drug molecules that show significant differences in potency among their enantiomers and racemic compounds.[31] Similarly, these differences in crystal domains can also have a significant effect on the conductive properties of organic materials. Pu et al. found that the median current of oligo(arylene−ethynylene) devices could be enhanced by up to 80-fold by using a homochiral material as opposed to racemic versions of the same compound.[32] Hatakeyama et al. have shown photoinduced charge transport in bulk films of azaboradibenzo[6]helicene is sensitive to chiral composition.[33]

Conductive properties of poly(alkoxythiophenes) are known to be influenced by their crystalline properties. Lovinger et al. found that conductivity in α-hexathienyl was influenced by crystal size.[34] Aiyar et al. established the relationship between the degree of crystallinity and charge transport in poly(3-hexylthiophene) (P3HT),[35] while Wang et al. were able to control the crystallization of P3HT to decrease the exciton bandwidth and increase its hole mobility.[36] Thus, it has been well established that chirality and the associated crystalline properties can influence biological activity and conductive properties that are relevant for the development of EDOT-MA and its associated polymer as a conductive biomaterial.

1.2. Chirality in Biological Systems. Chirality is known to have a significant impact on the macroscopic properties of both small molecules and polymers.[37] Chirality affects the efficacy of biological processes, resulting in profound effects on drug delivery,[38] biointerfacing,[39] and biocompatibility.[40]

Natural proteins and their constituent amino acids are intrinsically chiral. They are known to specifically recognize chiral substrates and receptors in biological systems. The attachment, spreading, proliferation, and differentiation of cells is highly associated with chirality.[41] For example, Addadi et al. did important studies in this regard, looking at the interactions of antibodies with chiral crystals.[42−45] They found that certain antibody 48E selectively bound to the $(0\bar{1}1)$ face of the (L)leu−(L)leu−(L)tyr protein crystal but did not bind to the (D)leu−(D)leu−(D)tyr crystals. Through theoretical modeling, they determined that the chiral recognition was a function of the geometric configuration of the binding sites. If the geometric configuration was suitable, H-bonding groups andhydrophobic groups on the antibody binding sites would interact with the carboxylic groups, amine groups, and hydrophobic side groups on the surface of the crystal, thus giving chirally selective antibody interactions.

Separate studies have found that cell adhesion, growth, spread, and assembly can be chirality dependent.[46−48]

In addition to examples of chirality influencing biological processes, there is also some evidence of chirality having a direct impact on interactions with neurological cells and tissues. Baranes et al.[49] demonstrated that D-cysteine significantly promotes neuronal growth and attachment to surfaces as compared to L-cysteine, which has a retarding effect.

1-Hydroxy-3-aminopyrrolidone-2 (HA-966) is a chiral drug used for a variety of central nervous system actions, including anticonvulsion, antitremor, muscle relaxant, and antimyclonic effects, among others.[50,51] (−)HA-966 enantiomer required a tenth of the dose as compared to (+)HA-966 enantiomers to block neuronal impulse flow receptors and elevate dopamine levels in the forebrains of rats.

These studies demonstrate the importance of understanding and controlling the chirality of organic and biomolecular materials.

In our previous paper, we synthesized a racemic compound (with both *R* and *S* enantiomers) of EDOT-MA.[19] In this paper, we demonstrate the synthesis of a homochiral version of EDOT-MA consisting of only the *S* enantiomer. We also characterize the crystal structure of both the racemic and homochiral compounds. We compare the crystallographic properties of both the homochiral and racemic EDOT-MA samples using optical and electron microscopy, powder X-ray diffraction (XRD), single-crystal XRD, and differential scanning calorimetry (DSC). As we show, the ability to control the monomer chirality has a dramatic impact on the symmetry of the crystal unit cell as well as the size and shape of the crystals that were formed when precipitated from dilute solutions.

2. MATERIALS AND METHODS

3,4-dimethoxythiophene, (*R*)-3-chloro-1,2-propanediol, triphenylphosphine, maleic anhydride, and *p*-toluenesulfonic acid were purchased from Sigma-Aldrich Chemicals and were used as received. Sodium sulfate, sodium azide, glacial acetic acid, sodium hydroxide, and hydrochloric acid were procured from Thomas Baker Ltd., Mumbai, India, and were used as received. All solvents were of reagent grade and were purified according

https://doi.org/10.1021/acsomega.3c07719
ACS Omega 2024, 9, 13655−13665

Scheme 1. Reaction Schematic for Homochiral EDOT-MA Synthesis

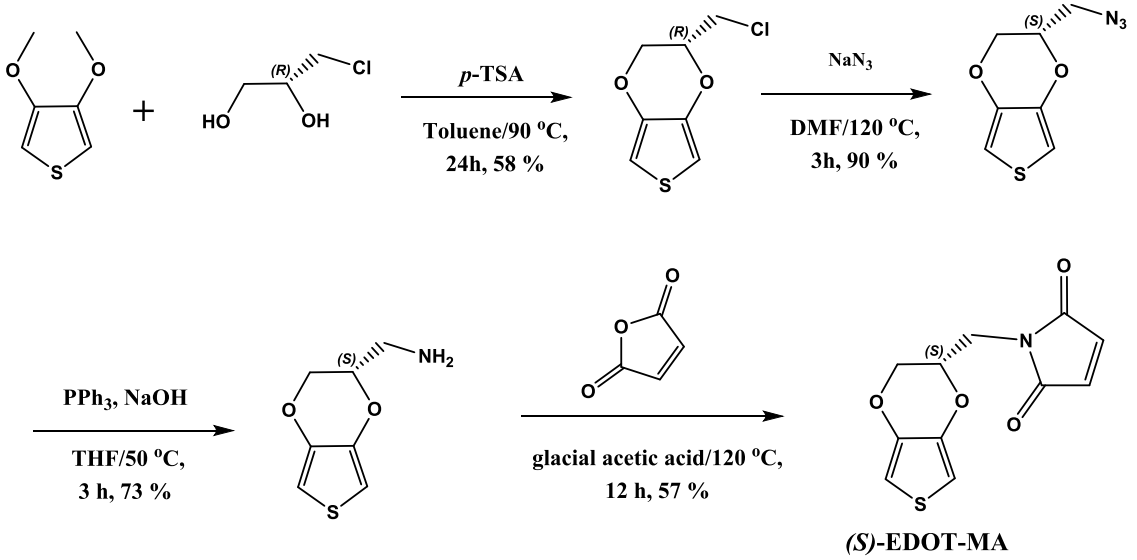

to standard procedures. Synthesis of the racemic EDOT-MA monomers has been conducted in the past by us using the 3,4-dimethoxythiophene as a precursor. We introduced chirality into our molecule by reacting the 3,4-dimethoxythiophene with chirally pure (*R*)-3-chloro-1,2-propanediol to give us the chiral chlorine-functionalized EDOT product. We further converted this into chiral (2-azidomethyl-2,3-dihydrothienol-[3,4-*b*][1,4]dioxin (EDOT-azide) and 2,3-dihydrothieno[3,4-*b*][1,4]dioxin-2-yl)methanamine (EDOT-amine) before finally reacting it with the maleic anhydride to obtain the homochiral EDOT-MA. The reaction scheme is described in Scheme 1. The detailed synthetic procedures are given below.

2.1. Characterization Methods. NMR spectra were recorded on a Bruker 400 MHz spectrometer at resonance frequencies of 400 MHz for ^{1}H NMR and 100 MHz for ^{13}C NMR measurements using $CDCl_3$ as a solvent. Attenuated total reflectance−Fourier transform infrared (ATR−FTIR) spectra of thiophene monomers were recorded on a PerkinElmer Spectrum 100 ATR−FTIR spectrometer.

Polarized optical microscopy images were acquired in transmitted white light by using a Nikon-Eclipse LVPOL100 with a full-wave red filter.

Differential scanning calorimetry was done using a Discovery DSC at the Advanced Materials Characterization Lab at the University of Delaware. Three DSC cycles were conducted from − 80 to 150 °C at a ramp rate of 10 °C/min for both the heating and the cooling cycles.

Scanning electron microscopy was performed using a Zeiss Auriga 60 focused ion beam−scanning electron microscope (FIB−SEM) operating at 1 kV.

Powder X-ray diffraction was performed on a Bruker D8 diffractometer in a symmetric $\theta/2\theta$ reflection geometry using monochromated CuKα radiation (λ = 1.54 Å) with 2θ ranging from 5 to 70°. Mercury 3.0 software was used to simulate powder X-ray spectra.[52]

Unit cell visualization and projections were done using Mercury 3.0. and Vesta 3.

Wide-angle (Figure S1) and small-angle X-ray (Figure S2) scattering (WAXS and SAXS) were performed on a Xeuss 2.0 HR SAXS/WAXS. The X-ray source was Cu Kα with a wavelength of 1.54 Å. The sample-to-detector distance was 75 mm for WAXS and 1200 mm for SAXS. The acquisition time of WAXS and SAXS was 5 and 30 min, respectively. Kapton tape was used to seal the samples into the sample holder.

ATR−FTIR spectra for the compounds (Figure S3) were recorded on a PerkinElmer Spectrum 100 FTIR after averaging 64 scans.

Single-crystal X-ray diffraction was performed by mounting the crystals using viscous oil onto plastic mesh at the data collection temperature on a Bruker-AXS D8 Venture Photon III diffractometer with CuKα radiation (λ = 1.54178 Å) focused with Goebel mirrors for the racemic crystal and on a Bruker-AXS APEX II DUO CCD diffractometer with graphite-monochromated MoKα radiation (λ = 0.71073 Å) for the homochiral crystal. Unit cell parameters were obtained from 36 data frames, 0.5° ω, from three different sections of the Ewald sphere.[53] The unit cell parameters, systematic absences in the data, and equivalent reflections were consistent with $P3_1$ and $P3_2$ for the homochiral case and, uniquely, with $P2_1/c$ for the racemic crystal. Refinement of the absolute structure parameter to nil within experimental error indicates the true hand of the data was determined in $P3_1$. The data was then treated with multiscan absorption correction, and the structure was solved using intrinsic phasing methods and refined with full matrix least squared procedures on F^2.[54] Non-hydrogen atoms were refined using anisotropic displacement parameters. The maleimide hydrogens were located from the electron density difference map and were allowed to refine freely. All other hydrogens were treated as idealized contributions with geometrically calculated positions and with U_{iso} equal to 1.2 U_{eq} of the attached atom. Atomic scattering factors are contained in the SHELXTL program library.[55] For the homochiral case: CCDC 2262792; 15192 reflections were measured ($5.288° \leq 2\theta \leq 63.01°$), out of which 3554 were unique (R_{int} = 0.0269, R_{sigma} = 0.0217), which were used in all calculations. The final R_1 was 0.0237 ($I > 2\sigma(I)$), and wR_2 was 0.0616 (all data). For the racemic case: CCDC 2262811; 1815 reflections were measured ($7.274° \leq 2\theta \leq 130.14°$), out of which 1815 were unique (R_{int} = 0.0339, R_{sigma} = 0.0196), which were used in all calculations. The final R_1 was 0.0314 ($I > 2\sigma(I)$), and wR_2 was 0.0784 (all data)

https://doi.org/10.1021/acsomega.3c07719
ACS Omega 2024, 9, 13655−13665

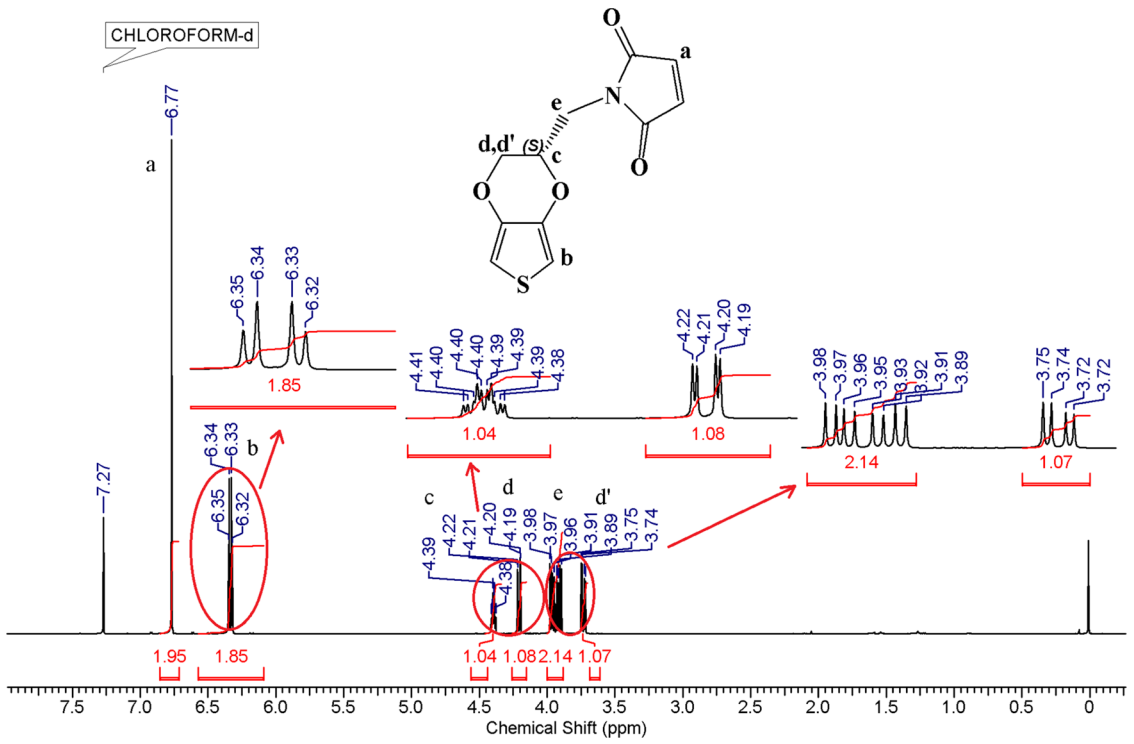

Figure 1. ^{1}H NMR spectrum of (*S*)-EDOT-MA.

2.2. Synthesis of *S*-EDOT-Maleimide: (*S*) EDOT-MA. The formation of (*R*)-EDOT-Cl is the first step of the reaction. For that, 3, 4-dimethoxythiophene and (*R*)-3-chloro-1,2-propanediol were mixed, and the reaction was catalyzed using *p*-toluenesulfonic acid (*p*-TSA) to yield (*R*)-EDOT-Cl. The next step involved the conversion of (*R*)-EDOT-Cl into (*S*) EDOT-N_3. This was achieved by nucleophilic substitution of the chloride group with sodium azide, with DMF used as the solvent. The next step involved the conversion of (*S*) EDOT-N_3 into (*S*) EDOT-NH_2 through a reduction reaction with triphenylphosphine and sodium hydroxide. In the final step, (*S*) EDOT-NH_2 was reacted with maleic anhydride in glacial acetic acid to give us the (*S*) EDOT-MA. Purification was done using column chromatography, followed by recrystallization from petroleum ether/ethyl acetate (70:30, v/v).

2.2.1. Synthesis of (R)-EDOT-Cl. A 500 mL two-neck round-bottom flask with a reflux condenser and argon inlet was set up. 3,4-Dimethoxythiophene (15.0 g, 104.02 mmol), anhydrous toluene (300 mL) with (*R*)-3-chloro-1,2-propanediol (23.57 g, 231.24 mmol), and *p*-toluenesulfonic acid (*p*-TSA) (1.79 g, 10.40 mmol) were added to the flask. The reaction mixture was then stirred at 90 °C for 24 h. After 24 h, (*R*)-3-chloro-1,2-propanediol (23.57 g) was further added to the mixture. This reaction mixture was allowed to stir at 90 °C for a further 3 h, after which it was allowed to quench to room temperature, and the solvent was removed under vacuum. A 10% sodium bicarbonate (200 mL) solution was added to this crude mixture, and the (*R*)-EDOT-Cl was extracted using dichloromethane (3 × 200 mL). Then, the organic phases were combined and washed with water (2 × 200 mL) before being dried over anhydrous sodium sulfate, filtered, and evaporated under vacuum. The filtrate was then purified by column chromatography using a petroleum ether/dichloromethane mixture (50:50, v/v) to give us (*R*)-EDOT-Cl (11.54 g, 58%).

^{1}H NMR (400 MHz, $CDCl_3$): δ = 6.37 (dd, 2H), 4.40−4.37 (m, 1H), 4.28 (dd, 1H), 4.16 (dd, 1H), 3.73−3.65 (m, 2H), ^{13}C NMR: δ = 141.0, 140.5, 100.0, 72.7, 65.4, 41.2 ppm.

2.2.2. Synthesis of (S) EDOT-N_3. Similar to the previous step, a 500 mL two-neck round-bottom flask equipped with a reflux condenser and argon inlet was set up. (*R*)-EDOT-Cl (10.0 g, 52.45 mmol) was added along with *N*,*N*-dimethylformamide (150 mL) to the flask. Following this, sodium azide (6.82 g, 104.91 mmol) was added, and the reaction mixture was allowed to stir at 120 °C for 3 h. Following this, the mixture was allowed to cool to room temperature, and the *N*,*N*-dimethylformamide was then removed using rotary evaporation under vacuum. Following this step, excess water (300 mL) was added to the residue in preparation for extraction. The product was then extracted using diethyl ether (2 × 250 mL). A pale yellow oily liquid (9.32 g, 90%) of (*S*) EDOT-N_3 was obtained after the solution was dried over anhydrous sodium sulfate, followed by filtration, and evaporated under reduced pressure.

^{1}H NMR (400 MHz, $CDCl_3$): δ = 6.39 (dd, 2H), 4.34−4.30 (m, 1H), 4.20 (dd, 1H), 4.05 (dd, 1H), 3.61−3.48 (m, 2H), ^{13}C NMR: δ = 141.0, 140.6, 100.2, 100.1, 72.4, 65.7, and 50.5 ppm.

2.2.3. Synthesis of (S) EDOT-NH_2. A 500 mL two-neck round-bottom flask with a reflux condenser and a magnetic stirring bar was set up. Tetrahydrofuran (100 mL), (*S*) EDOT-N_3 (9.0 g, 45.64 mmol), triphenylphosphine (14.36 g, 54.76 mmol), and 2 mol L^{-1} sodium hydroxide aqueous solution (100 mL) were added to this flask, and the reaction mixture was allowed to stir at 50 °C for 3 h. The mixture was then quenched to room temperature. The tetrahydrofuran was then evaporated, and a 2 M hydrochloric acid solution was used to keep the pH of the mixture below 3. Extraction was done from the aqueous layer using dichloromethane (2 × 100 mL), and the combined organic layers were discarded. A 1 M sodium

https://doi.org/10.1021/acsomega.3c07719
ACS Omega 2024, 9, 13655−13665

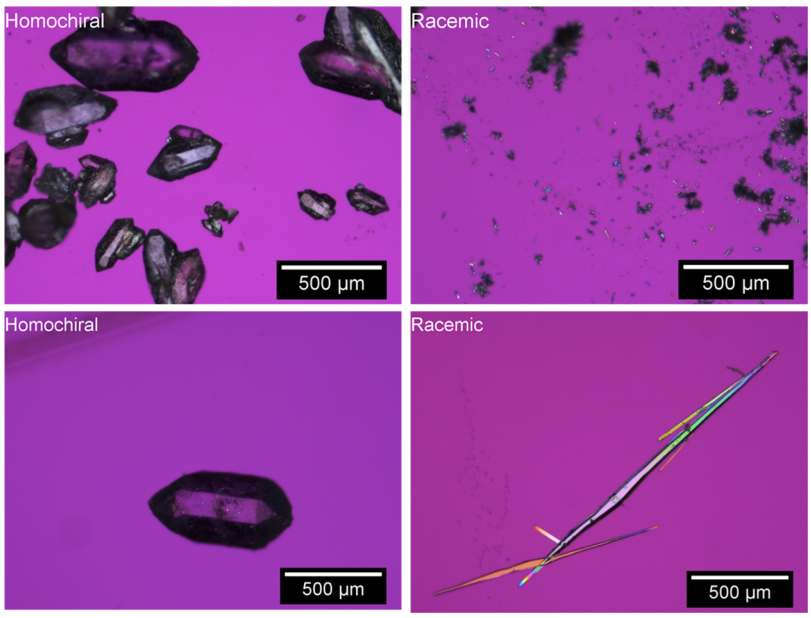

Figure 2. (*S*) homochiral (left) and racemic (*R*,*S*) (right) crystals of EDOT-MA under a polarized optical microscope with a full-wave red filter.

hydroxide solution was added to the aqueous part to adjust the pH to 12. The second extraction of the aqueous layer using dichloromethane (3 × 100 mL) was performed at this pH. The organic layer was dried with anhydrous sodium sulfate, and the solvent was removed under vacuum to give us (*S*) EDOT-NH_2 as a colorless oil (5.71 g, 73%).

^{1}H NMR (400 MHz, $CDCl_3$): δ = 6.33 (dd, 2H), 4.20 (dd, 1H), 4.12 (m, 1H), 4.00 (dd, 1H), 2.97 (m, 2H), 1.32 (s, 2H) ^{13}C NMR: δ = 141.6, 140.5, 99.5, 75.2, 66.6, and 42.3 ppm.

2.2.4. Synthesis of (S) EDOT-MA. For the final synthesis step, a 250 mL two-neck round-bottom flask equipped with a mechanical stirrer, a gas inlet, and a reflux condenser was used. (*S*) EDOT-NH_2 (5.0 g, 29.20 mmol), maleic anhydride (3.44 g, 35.04 mmol), and glacial acetic acid (100 mL) were added to the flask. The reaction mixture was then stirred at 120 °C for 12 h before being cooled to room temperature. The glacial acetic acid was removed by evaporation under vacuum. The product was then dissolved in ethyl acetate and washed with water (3 × 50 mL). This ethyl acetate solution was then dried over anhydrous sodium sulfate, followed by filtration and evaporation under vacuum to remove the ethyl acetate. The obtained crude product was then purified using column chromatography with petroleum ether/ethyl acetate (70:30, v/v) as the mobile phase to give us purified (*S*) EDOT-MA (4.16 g, 57%).

FTIR: 1704 cm^{-1}; ^{1}H NMR (400 MHz, $CDCl_3$): δ = 6.77 (s, 2H), 6.34 (dd, 2H), 4.40 (td, 1H), 4.21 (dd, 1H), 3.98−3.89 (dddd, 2H), 3.74 (dd, 1H); ^{13}C NMR (100 MHz, $CDCl_3$): δ = 170.2, 141.0, 134.3, 100.2, 70.9, 66.1, 37.7 ppm. Melting point (DSC) was 128.6 °C (Figure 1).

3. RESULTS AND DISCUSSION

3.1. Solution Crystallization. Homochiral EDOT-MA readily crystallized from a 1:1 ethyl acetate−petroleum ether solvent mixture, forming large single crystals at times visible to the naked eye. These crystals showed high birefringence, as seen in the polarized optical micrographs. The higher refractive index direction was along the longer axis of the crystals.

Racemic EDOT-MA crystals, on the other hand, were grown in a closed chamber over 3 months from a 1:2 acetonitrile in water solution. The chamber was sealed with a rubber cork and a fine 20-gauge needle to allow for slow solvent evaporation. Large needle-like crystals were formed, which showed birefringence, with the higher refractive index direction along the orientation of the needle.

The racemic EDOT-MA crystal structure has been deposited at the Cambridge Structural Database under CCDC 2262811. The homochiral (*S*) EDOT-MA crystal structure was deposited under CCDC 2262792.

3.2. Optical Microscopy. Polarized optical microscopy images of homochiral EDOT-MA confirmed their single-crystal nature. The crystals were often several hundred micrometers in length and showed a consistent hexagonal shape with tapered tips. Clear evidence of anisotropic birefringence was seen under crossed polars with a full-wave red filter. The color of the crystal remained uniform throughout when the sample stage was rotated, indicating that the relative orientation of the molecules was consistent within a given crystal domain. The images showed clean symmetric hexagonal single crystals tapering on both ends along their length (Figure 2). The typical size of the single crystals varied from 50 to 600 μm in length, with relatively small aspect ratios (L/D) between 1 and 5.

The racemic single crystals, on the other hand, had high aspect ratios (L/Ds of 50 or more) with a much more needle-like shape (Figure 2). Although some crystals were quite long and visible to the naked eye (more than 1 mm), their typical size was much smaller than that of the homochiral samples. Anisotropic birefringence was observed for these crystals as well. Racemic crystals were typically more brittle than the homochiral crystals, possibly due to their higher aspect ratio.

3.3. Single-Crystal X-ray Diffraction. Individual crystals were isolated from both the homochiral (*S*) EDOT-MA and racemic (*R*,*S*) EDOT-MA samples, and the crystal structures were determined using single-crystal X-ray diffraction. The results are summarized in Table 1, and the CIF files with

https://doi.org/10.1021/acsomega.3c07719
ACS Omega 2024, 9, 13655−13665

atomic coordinates are included in the Supporting Information.

Table 1. (*S*) EDOT-MA Homochiral and EDOT-MA-Racemic Unit Cell Descriptions

name	homochiral (*S*) EDOT-MA	racemic EDOT-MA
temperature of measurement (K)	120	100
crystal system	trigonal	monoclinic
space group	$P3_1$ (No. 144)	$P2_1/c$
a (Å)	8.8959 (13)	12.7721 (7)
b (Å)	8.8959 (13)	6.0118 (3)
c (Å)	11.662 (2)	14.7151 (8)
α (°)	90	90
β (°)	90	107.897 (2)
γ (°)	120	90
volume (Å^3)	799.3 (3)	1075.2 (10)
Z	3	4
density$_{calc}$ (g/cm^3)	1.566	1.552
M (mm^{-1})	0.305	2.736
F(000)	390.0	520.0
crystal dimensions (mm^3)	0.445 × 0.313 × 0.148	0.179 × 0.066 × 0.042
radiation	Mo−Kα (λ = 0.71073)	Cu−Kα (λ = 1.54178)
2θ range for data collection (°)	5.288−63.01	7.274−130.14

There is a distinctive difference between the unit cells of both the racemic and homochiral crystals (seen in Figure 3). The homochiral crystal forms a 3-fold helix along the *c*-axis, with the maleimide units extended to the side of the helix and the maleimide groups pushed outward. Comparatively, the racemic version has four EDOT-MA molecules in inverted pairs, with the maleimide units parallel to the EDOT molecule. The homochiral crystals show the *S*-symmetry of the chiral center and are oriented in a polar fashion, with the maleimide units all pointing in the same direction (along [001]).

Looking at the organization of the EDOT-MA molecules within the unit cell for both structures, we can see that the local packing is heavily influenced by steric effects caused by the maleimide functional group. The inversion in the racemic molecules and the helicity in the homochiral variant have the effect of reducing steric interactions between the maleimide functional groups. Also, the conformations of the EDOT-MA molecule are substantially different in the two polymorphs. In the homochiral crystal, the maleimide side group is sticking out to one side of the alkoxy-thiophene, creating a shape approximately similar to that of the capital letter "L" (Figure 3a). Because of the controlled chirality, all of the molecules in the homochiral crystal have the same overall shape. On the other hand, the overall conformations of the EDOT-MA units in the racemic crystals are more colinear, with the maleimide and the alkoxy-thiophene rings nearly aligned (Figure 3b). There is a crystalline inversion center between each neighboring pair of molecules, and hence, chirality alternates between molecules as we go down a line as *R*-*S*-*R*-*S* and so on.

It is to be noted that we found that the homochiral EDOT-MA molecule was found to pack in the chiral space group #144 ($P3_1$), which can accommodate the right-handed symmetry of the 3-fold helices that the molecules are seen to adopt in the solid state. We expect that the EDOT-MA with the opposite handedness, i.e., EDOT-MA (*R*) would adopt helices of the opposite (left) handedness, and thus would be expected to adopt the space group that is the enantiomeric pair of #144: #145, or $P3_2$.[56] At the moment, the EDOT-MA (*R*) molecule is difficult to synthesize because of the limited availability of the corresponding chiral starting reagents. However, this possibility can be evaluated in the future and seems to be reasonable based on symmetry considerations alone.

In previous studies of carboxylic acid functionalized EDOT (EDOT-acid), we found that the solid-state packing was dominated by hydrogen bonding between side groups.[57] No such hydrogen bonding is possible in these maleimide-functionalized compounds. This contrast tells us that the stereochemistry of the functional group has a strong effect on the packing of the monomers. Additionally, the maleimide functional groups have a strong steric effect such that they dominate effects with van der Waals forces, unlike the polar carboxylic acid functional group.

The theoretical densities of the homochiral (*S*) and racemic (*R*,*S*) EDOT-MA crystals determined by single-crystal X-ray diffraction were nearly equivalent: 1.566 and 1.552 g/cm^3, respectively. These densities are higher than the density of unsubstituted EDOT (1.42 g/cm^3) and just slightly lower than the density of EDOT-acid crystals (1.63 g/cm^3).[57] The unit cell of EDOT-acid has eight molecules with orthorhombic symmetry, with hydrogen bonds formed between carboxylic acid dimers in the solid state. This presumably leads to its slightly higher density. No such effects are expected in unsubstituted EDOT or in EDOT-MA. Thus, we can estimate that the average intermolecular forces in homochiral EDOT-

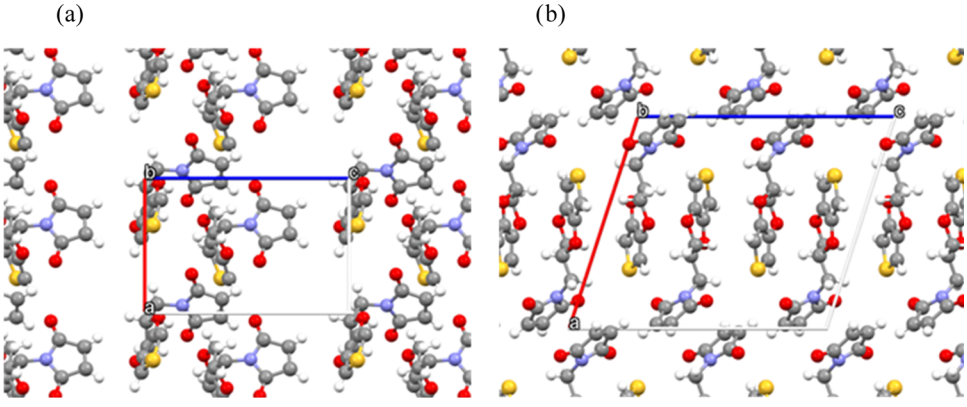

Figure 3. Projections of unit cells in the *b* [010] direction: (a) (*S*) EDOT-MA, (b) EDOT-MA.

https://doi.org/10.1021/acsomega.3c07719
ACS Omega 2024, 9, 13655−13665

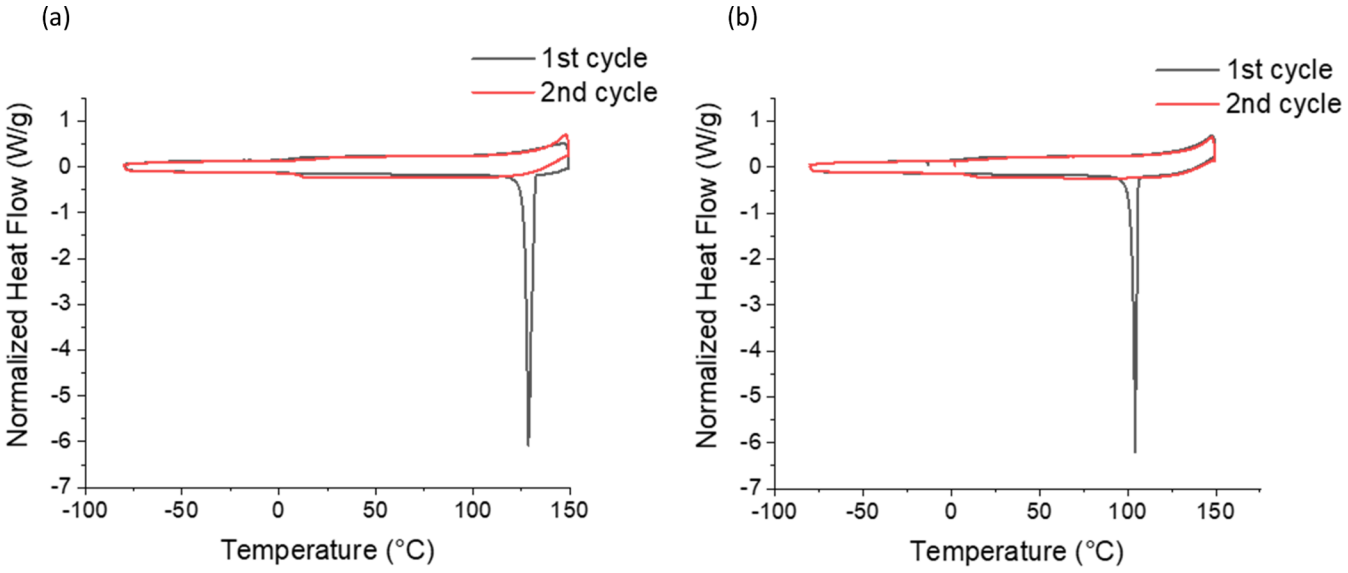

Figure 4. Differential scanning calorimetry scans for homochiral (a) (*S*) EDOT-MA and (b) racemic (*R*,*S*) EDOT-MA. The homochiral sample melts at 128.6 C, whereas the racemic sample melts at 104.2 C.

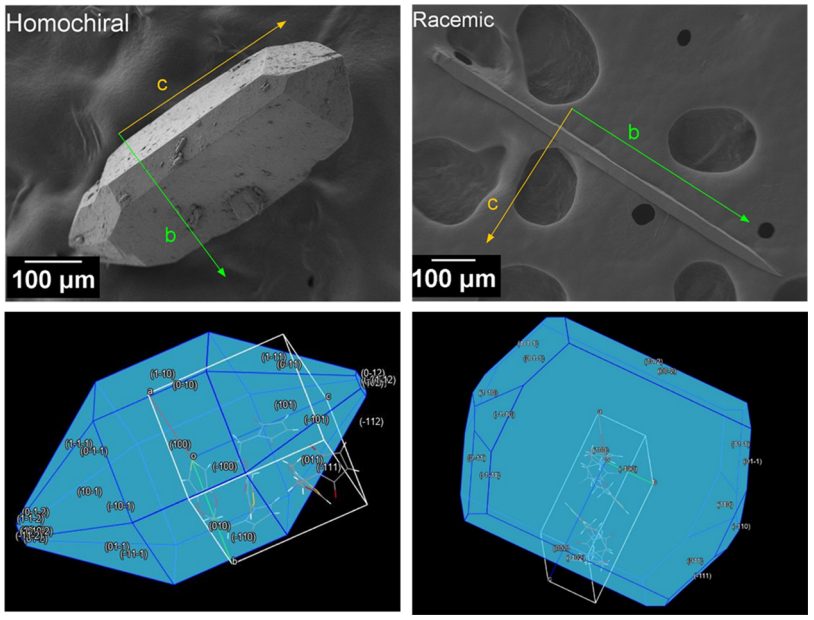

Figure 5. Top panels: SEM Images of single crystal and with facets: homochiral (*S*) EDOT-MA (left) and racemic (*R*,*S*) EDOT-MA (right). Bottom panels: Theoretical simulations of crystal shape were obtained using the BFDH analysis from Mercury software.

MA are stronger than those in EDOT but weaker than those in EDOT-acid. This hypothesis is supported also by the fact that homochiral EDOT-MA melts at 128.6 °C, which is slightly lower than the melting temperature of EDOT-acid (139 °C) (Figure S4). On the other hand, unsubstituted EDOT melts below room temperature at about 10 °C.

3.4. EDOT-MA Thermal Analysis. During the first heating cycle of the DSC, a sharp melting peak was seen with a peak temperature of 128.6 °C for the homochiral EDOT-MA molecule, with no observable glass transition occurring (Figure 4a). Notably, we saw no recrystallization peaks during any of the three cooling cycles. During the second and third heating cycles, however, we noticed the appearance of a glass transition without a melting peak, indicating that the heating cycle had changed the material from primarily crystalline to primarily amorphous. The midpoint for the glass transition in the second heating cycle was at 10.1 °C, while it was at 23.4 °C for the third heating cycle. This indicated that the thermal treatment was causing some subtle changes in the macroscopic properties of the material.

A similar effect was seen in the racemic molecules as well. Interestingly, the controlled chirality of the molecules had a significant impact on the melting points of these crystals, with the racemic molecules melting at 104.2 °C (Figure 4b) compared to 128.6 °C for the homochiral molecule. This indicates that the change in chirality impacts the intermolecular binding forces for EDOT-MA, with the homochiral crystals showing stronger binding forces.

3.5. Scanning Electron Microscopy. SEM images of the EDOT-MA single crystals were taken at an accelerating voltage

https://doi.org/10.1021/acsomega.3c07719
ACS Omega 2024, 9, 13655−13665

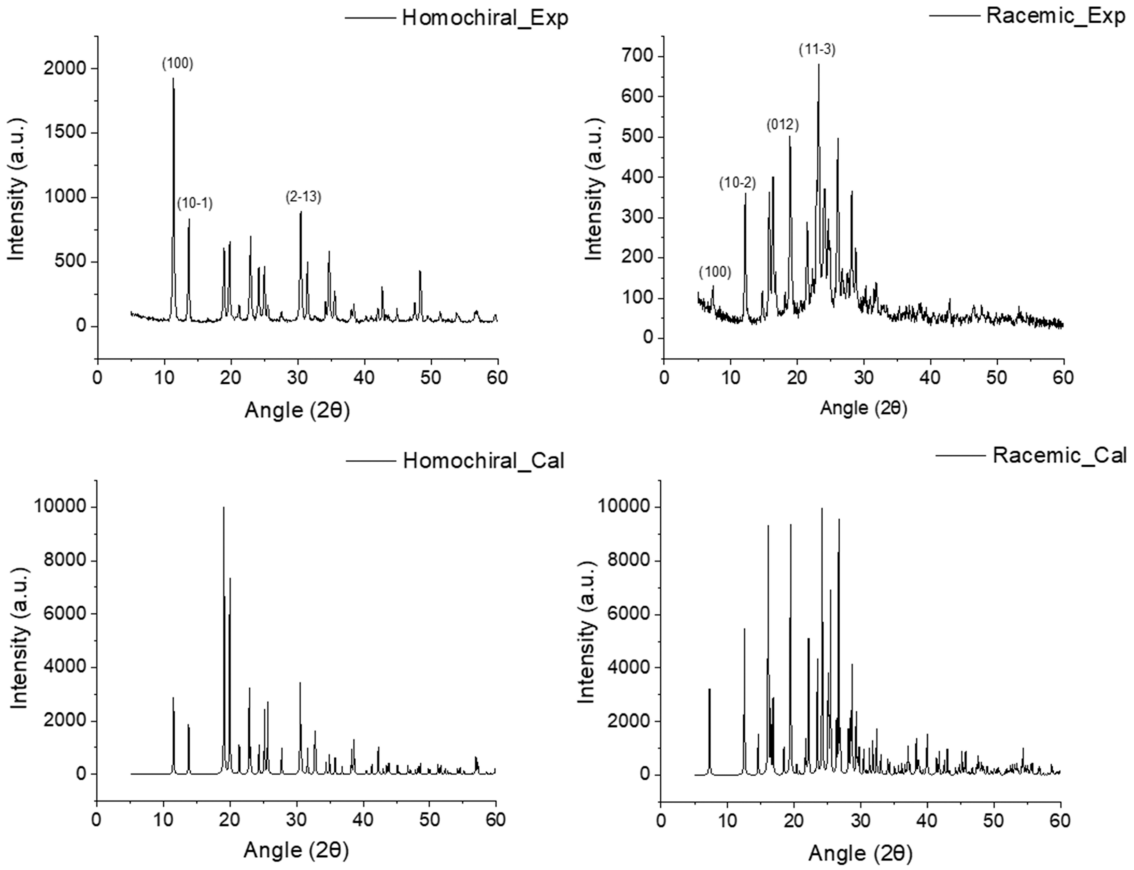

Figure 6. Top panels: experimental powder XRD spectra for the homochiral (*S*) EDOT-MA (left) and racemic (*R*,*S*) EDOT-MA (right). Bottom panels: Mercury 3.0 powder diffraction calculations for single-crystal unit cell homochiral (*S*) EDOT-MA (left) and racemic (*R*,*S*) EDOT-MA (right).

of 1 kV after mounting the crystals on carbon tape to minimize charging. We were able to clearly see the various facets of the crystals in the SEM (Figure 5). The shapes of the crystals were consistent with simulations predicted using Bravais−Friedel−Donnay−Harker (BFDH) analysis with Mercury 3.0 software.

3.6. Crystal Morphology. From the SEM and OM observations and the single-crystal X-ray structures and BFDH shape simulations, it is possible to assign the external facets seen in individual crystals to crystallographic orientations. The trigonal homochiral (*S*) EDOT-MA crystals have their *c*-axis parallel to the long axis of the crystal, while for the monoclinic, racemic (*R*,*S*) EDOT-MA crystals, the *b*-axis is oriented along the longest crystal axis (Figure 5). The trigonal homochiral crystals have their (100) planes perpendicular to the *a* and *b* axes, forming predominant lateral faces of the crystal, while the (101) type planes form the facets on the tapered crystal ends. The monoclinic racemic (*R*,*S*) EDOT-MA crystals have (100) type crystal faces in the *a*-direction; while (002) type faces are present perpendicular to the *c*-axis, making up the lateral planes of the crystal. There are (110), $(11\bar{1})$, and $(01\bar{1})$ type planes along the longitudinal *b*-axis.

3.7. Powder X-ray Diffraction. The positions of the observed peaks as well as the absence of the simulated patterns (Mercury 3.0) were consistent with those of the experimental powder patterns. The reflections for the planes corresponding to the single crystals could be clearly identified in the experimental results (Figure 6). This further confirms that the single-crystal reflections obtained are compatible with the powder XRD results. Wide-angle X-ray diffraction (Figure S1) and small-angle X-ray diffraction (Figure S2) aligned well with the powder X-ray diffraction data.

4. CONCLUSIONS

In this paper, we were able to synthesize the homochiral version of EDOT-MA, (*S*) EDOT-MA. We characterized the solid-state structure of both homochiral (*S*) EDOT-MA and racemic (*R*,*S*) EDOT-MA in order to examine the effects of controlled chirality on the EDOT-MA unit cell crystal structure, crystal morphology, and thermal properties. The steric effects of the maleimide functional group dominated the local packing in these crystals. The (*R*,*S*) EDOT-MA racemic crystals were monoclinic, highly elongated, and much smaller than the homochiral (*S*) EDOT-MA variant under similar crystallization conditions. The (*S*) EDOT-MA homochiral crystals showed trigonal symmetry, with smaller aspect ratios, hexagonal shapes, and much larger sizes. Both crystals had similar densities, with the homochiral version only slightly denser. The homochiral (*S*) EDOT-MA crystals had somewhat higher melting points (T_m = 128.6 °C) than the racemic (*R*,*S*) EDOT-MA samples (104.2 °C). Both samples formed amorphous glasses after melting.

Our results show the impact of chirality control on the solid-state structure of these materials. We expect these results to be important in better understanding directing the solid-state assembly of the corresponding polymers prepared from these monomers.

https://doi.org/10.1021/acsomega.3c07719
ACS Omega 2024, 9, 13655−13665

■ ASSOCIATED CONTENT

Supporting Information

The Supporting Information is available free of charge at https://pubs.acs.org/doi/10.1021/acsomega.3c07719.

Further characterization data for the EDOT-MA crystals is provided as Supporting Information; including X-ray scattering and infrared spectroscopy; differential scanning calorimetry data for EDOT-acid is also provided (PDF)

Racemic EDOTMA_cif (CIF)

EDOTmalemide_s (CIF)

■ AUTHOR INFORMATION

Corresponding Author

David C. Martin − *Department of Materials Science and Engineering, University of Delaware, Newark, Delaware 19716, United States;* orcid.org/0000-0003-1195-3838; Email: milty@udel.edu

Authors

Shrirang S. Chhatre − *Department of Materials Science and Engineering, University of Delaware, Newark, Delaware 19716, United States;* orcid.org/0000-0003-3703-9104

Samadhan S. Nagane − *Department of Materials Science and Engineering, University of Delaware, Newark, Delaware 19716, United States*

Yuhang Wu − *Department of Materials Science and Engineering, University of Delaware, Newark, Delaware 19716, United States*

Junghyun Lee − *Department of Materials Science and Engineering, University of Delaware, Newark, Delaware 19716, United States;* orcid.org/0000-0001-7369-2384

Glenn P. A. Yap − *Department of Chemistry and Biochemistry, University of Delaware, Newark, Delaware 19716, United States;* orcid.org/0000-0003-0385-387X

Complete contact information is available at: https://pubs.acs.org/10.1021/acsomega.3c07719

Author Contributions

S.S.C.: Conceptualization, methodology, investigation, writing of original draft, editing, and review. S.N.: investigation, methodology, editing, and review. Y.W.: investigation, methodology, editing, and review. J.L.: editing and review. G.P.A.Y.: investigation, methodology, editing, and review. D.C.M.: conceptualization, resources, supervision, editing, and review.

Notes

The authors declare the following competing financial interest(s): The authors declare the following potential conflict of interest: the University of Delaware has filed a patent on Biofunctional thiophene monomers and polymers thereof for electronic biomedical devices, patent application PCT/US2020/048495, with inventors David C. Martin, Samadhan Nagane, and Peter Sitarik.

■ ACKNOWLEDGMENTS

This work was supported by the National Science Foundation (DMR-1808048) and by the University of Delaware. G.P.A.Y. thanks the National Institute of Health (S10-OD026896A).

■ REFERENCES

(1) Zhu, Z.-T.; Mabeck, J. T.; Zhu, C.; Cady, N. C.; Batt, C. A.; Malliaras, G. G. A Simple Poly(3,4-Ethylene Dioxythiophene)/Poly(Styrene Sulfonic Acid) Transistor for Glucose Sensing at Neutral PH. *Chem. Commun.* **2004**, No. No. 13, 1556.

(2) Lee, J.; Chhatre, S.; Sitarik, P.; Wu, Y.; Baugh, Q.; Martin, D. C. Electrochemical Fabrication and Characterization of Organic Electrochemical Transistors Using Poly(3,4-Ethylenedioxythiophene) with Various Counterions. *ACS Appl. Mater. Interfaces* **2022**, *14* (37), 42289−42297.

(3) Anothumakkool, B.; Soni, R.; Bhange, S. N.; Kurungot, S. Novel Scalable Synthesis of Highly Conducting and Robust PEDOT Paper for a High Performance Flexible Solid Supercapacitor. *Energy Environ. Sci.* **2015**, *8* (4), 1339−1347.

(4) Wu, Y.; Nagane, S. S.; Sitarik, P.; Chhatre, S.; Lee, J.; Martin, D. C. Capacitive Studies of Electrodeposited PEDOT-Maleimide. *J. Mater. Chem. A* **2022**, *10* (15), 8440−8458.

(5) Savagatrup, S.; Chan, E.; Renteria-Garcia, S. M.; Printz, A. D.; Zaretski, A. V.; O'Connor, T. F.; Rodriquez, D.; Valle, E.; Lipomi, D. J. Plasticization of PEDOT:PSS by Common Additives for Mechanically Robust Organic Solar Cells and Wearable Sensors. *Adv. Funct. Mater.* **2015**, *25* (3), 427−436.

(6) Sakata, T.; Ikeda, N.; Koganezawa, T.; Kajiya, D.; Saitow, K. Performance of Si/PEDOT:PSS Solar Cell Controlled by Dipole Moment of Additives. *J. Phys. Chem. C* **2019**, *123* (33), 20130−20135.

(7) Kawahara, J.; Ersman, P. A.; Engquist, I.; Berggren, M. Improving the Color Switch Contrast in PEDOT:PSS-Based Electrochromic Displays. *Org. Electron.* **2012**, *13* (3), 469−474.

(8) Blau, R.; Chen, A. X.; Polat, B.; Becerra, L. L.; Runser, R.; Zamanimeymian, B.; Choudhary, K.; Lipomi, D. J. Intrinsically Stretchable Block Copolymer Based on PEDOT:PSS for Improved Performance in Bioelectronic Applications. *ACS Appl. Mater. Interfaces* **2022**, *14* (4), 4823−4835.

(9) Fort, A.; Innocenti, M.; Foresti, M. L.; Mugnaini, M.; Pasquini, I.; Pigani, L.; Rocchi, S.; Vignoli, V.NO 2 QCM Gas Sensor Based on Electrochemical Deposition of PEDOT. In *2009 3rd International Workshop on Advances in sensors and Interfaces*; IEEE: Trani, Italy, 2009; pp 184−187 DOI: 10.1109/IWASI.2009.5184792.

(10) Martin, D. C.; Wu, J.; Shaw, C. M.; King, Z.; Spanninga, S. A.; Richardson-Burns, S.; Hendricks, J.; Yang, J. The Morphology of Poly(3,4-Ethylenedioxythiophene). *Polym. Rev.* **2010**, *50* (3), 340−384.

(11) Crispin, X.; Jakobsson, F. L.; Crispin, A.; Grim, P. C.; Andersson, P.; Volodin, A. V.; van Haesendonck, C. The Origin of the High Conductivity of Poly(3,4-Ethylenedioxythiophene)-Poly(Styrenesulfonate) (PEDOT-PSS) Plastic Electrodes. *Chem. Mater.* **2006**, *18* (18), 4354−4360.

(12) Asplund, M.; Thaning, E.; Lundberg, J.; Sandberg-Nordqvist, A. C.; Kostyszyn, B.; Inganäs, O.; von Holst, H. Toxicity Evaluation of PEDOT/Biomolecular Composites Intended for Neural Communication Electrodes. *Biomed. Mater.* **2009**, *4* (4), No. 045009.

(13) Martin, D. C. Molecular Design, Synthesis, and Characterization of Conjugated Polymers for Interfacing Electronic Biomedical Devices with Living Tissue. *MRS Commun.* **2015**, *5* (2), 131−153.

(14) Donahue, M. J.; Sanchez-Sanchez, A.; Inal, S.; Qu, J.; Owens, R. M.; Mecerreyes, D.; Malliaras, G. G.; Martin, D. C. Tailoring PEDOT Properties for Applications in Bioelectronics. *Mater. Sci. Eng., R* **2020**, *140*, No. 100546.

(15) Murbach, J. M.; Currlin, S.; Widener, A.; Tong, Y.; Chhatre, S.; Subramanian, V.; Martin, D. C.; Johnson, B. N.; Otto, K. J. In Situ Electrochemical Polymerization of Poly(3,4-Ethylenedioxythiophene) (PEDOT) for Peripheral Nerve Interfaces. *MRS Commun.* **2018**, *8* (3), 1043−1049.

(16) Tong, Y.; Murbach, J. M.; Subramanian, V.; Chhatre, S.; Delgado, F.; Martin, D. C.; Otto, K. J.; Romero-Ortega, M.; Johnson, B. N. A Hybrid 3D Printing and Robotic-Assisted Embedding Approach for Design and Fabrication of Nerve Cuffs with Integrated Locking Mechanisms. *MRS Adv.* **2018**, *3* (40), 2365−2372.

(17) Minudri, D.; Mantione, D.; Dominguez-Alfaro, A.; Moya, S.; Maza, E.; Bellacanzone, C.; Antognazza, M. R.; Mecerreyes, D. Water Soluble Cationic Poly(3,4-Ethylenedioxythiophene) PEDOT-N as a

Versatile Conducting Polymer for Bioelectronics. *Adv. Electron. Mater.* **2020**, *6* (10), No. 2000510.
(18) Yano, H.; Kudo, K.; Marumo, K.; Okuzaki, H. Fully Soluble Self-Doped Poly(3,4-Ethylenedioxythiophene) with an Electrical Conductivity Greater than 1000 S Cm^{-1}. *Sci. Adv.* **2019**, *5* (4), No. eaav9492.
(19) Nagane, S.; Sitarik, P.; Wu, Y.; Baugh, Q.; Chhatre, S.; Lee, J.; Martin, D. C. Functionalized Polythiophene Copolymers for Electronic Biomedical Devices. *MRS Adv.* **2020**, *5* (18−19), 943−956.
(20) Schelté, P.; Boeckler, C.; Frisch, B.; Schuber, F. Differential Reactivity of Maleimide and Bromoacetyl Functions with Thiols: Application to the Preparation of Liposomal Diepitope Constructs. *Bioconjugate Chem.* **2000**, *11* (1), 118−123.
(21) Lin, S.-C.; Wu, C.-S.; Yeh, J.-M.; Liu, Y.-L. Reaction Mechanism and Synergistic Anticorrosion Property of Reactive Blends of Maleimide-Containing Benzoxazine and Amine-Capped Aniline Trimer. *Polym. Chem.* **2014**, *5* (14), 4235−4244.
(22) Wang, Z.; Zhang, Y.; Zhang, H.; Harrington, P. B.; Chen, H. Fast and Selective Modification of Thiol Proteins/Peptides by N-(Phenylseleno) Phthalimide. *J. Am. Soc. Mass Spectrom.* **2012**, *23* (3), 520−529.
(23) Sitarik, P.; Nagane, S. S.; Chhatre, S.; Wu, Y.; Baugh, Q.; Martin, D. C. Synthesis and Characterization of Maleimide Functionalized Poly(3,4-Ethylenedioxythiophene) (PEDOT) Polymers. *Mater. Adv.* **2022**, *3* (14), 6037−6049.
(24) Chhatre, S. S. Molecular-Scale Analysis of the Polymerization of Poly (3, 4-Ethylenedioxythiophene)(PEDOT); University of Delaware 2022.
(25) Wu, Y.; Nagane, S. S.; Baugh, Q.; Lo, C.-Y.; Chhatre, S. S.; Lee, J.; Sitarik, P.; Kayser, L. V.; Martin, D. C. Cholesterol-Substituted 3,4-Ethylenedioxythiophene (EDOT-MA-Cholesterol) and Poly(3,4-Ethylenedioxythiophene) (PEDOT-MA-Cholesterol). *Giant* **2023**, *15*, No. 100163.
(26) Pasteur, L. *Researches on the Molecular Asymmetry of Natural Organic Products (No. 14)*; WF Clay, 1897; Vol. *14*.
(27) Moussa, H.; Jiang, W.; Alsheghri, A.; Mansour, A.; Hadad, A. E.; Pan, H.; Tang, R.; Song, J.; Vargas, J.; McKee, M. D.; Tamimi, F. High Strength Brushite Bioceramics Obtained by Selective Regulation of Crystal Growth with Chiral Biomolecules. *Acta Biomater.* **2020**, *106*, 351−359.
(28) Gal, J. The Discovery of Stereoselectivity at Biological Receptors: Arnaldo Piutti and the Taste of the Asparagine Enantiomers-History and Analysis on the 125th Anniversary: PIUTTI, THE ASPARAGINE ENANTIOMERS, SWEET TASTE, AND RECEPTORS. *Chirality* **2012**, *24* (12), 959−976.
(29) Brandt, J. R.; Salerno, F.; Fuchter, M. J. The Added Value of Small-Molecule Chirality in Technological Applications. *Nat. Rev. Chem.* **2017**, *1* (6), 0045.
(30) Perlovich, G. L.; Kurkov, S. V.; Hansen, L. Kr.; Bauer-Brandl, A. Thermodynamics of Sublimation, Crystal Lattice Energies, and Crystal Structures of Racemates and Enantiomers: (+)- and (±)-Ibuprofen. *J. Pharm. Sci.* **2004**, *93* (3), 654−666.
(31) Hancu, G.; Modroiu, A. Chiral Switch: Between Therapeutical Benefit and Marketing Strategy. *Pharmaceuticals* **2022**, *15* (2), 240.
(32) Zhu, Y.; Gergel, N.; Majumdar, N.; Harriott, L. R.; Bean, J. C.; Pu, L. First Optically Active Molecular Electronic Wires. *Org. Lett.* **2006**, *8* (3), 355−358.
(33) Hatakeyama, T.; Hashimoto, S.; Oba, T.; Nakamura, M. Azaboradibenzo[6]Helicene: Carrier Inversion Induced by Helical Homochirality. *J. Am. Chem. Soc.* **2012**, *134* (48), 19600−19603.
(34) Lovinger, A. J.; Davis, D. D.; Dodabalapur, A.; Katz, H. E.; Torsi, L. Single-Crystal and Polycrystalline Morphology of the Thiophene-Based Semiconductor R-Hexathienyl (R-6T). *Macromolecules* **1996**, *29* (14), 4952−4957.
(35) Aiyar, A. R.; Hong, J.-I.; Nambiar, R.; Collard, D. M.; Reichmanis, E. Tunable Crystallinity in Regioregular Poly(3-Hexylthiophene) Thin Films and Its Impact on Field Effect Mobility. *Adv. Funct. Mater.* **2011**, *21* (14), 2652−2659.
(36) Wang, G.; Persson, N.; Chu, P.-H.; Kleinhenz, N.; Fu, B.; Chang, M.; Deb, N.; Mao, Y.; Wang, H.; Grover, M. A.; Reichmanis, E. Microfluidic Crystal Engineering of π-Conjugated Polymers. *ACS Nano* **2015**, *9* (8), 8220−8230.
(37) Qing, G.; Sun, T. The Transformation of Chiral Signals into Macroscopic Properties of Materials Using Chirality-Responsive Polymers. *NPG Asia Mater.* **2012**, *4* (1), e4.
(38) Agranat, I.; Caner, H.; Caldwell, J. Putting Chirality to Work: The Strategy of Chiral Switches. *Nat. Rev. Drug Discovery* **2002**, *1* (10), 753−768.
(39) Zhang, M.; Qing, G.; Sun, T. Chiral Biointerface Materials. *Chem. Soc. Rev.* **2012**, *41* (5), 1972−1984.
(40) He, H.; Zhang, L.; Guan, X.; Cheng, H.; Liu, X.; Yu, S.; Wei, J.; Ouyang, J. Biocompatible Conductive Polymers with High Conductivity and High Stretchability. *ACS Appl. Mater. Interfaces* **2019**, *11* (29), 26185−26193.
(41) Hynes, R. O. The Extracellular Matrix: Not Just Pretty Fibrils. *Science* **2009**, *326* (5957), 1216−1219.
(42) Perl-Treves, D.; Kessler, N.; Izhaky, D.; Addadi, L. Monoclonal Antibody Recognition of Cholesterol Monohydrate Crystal Faces. *Chem. Biol.* **1996**, *3* (7), 567−577.
(43) Izhaky, D.; Addadi, L. Pattern Recognition by Antibodies for Two-Dimensional Arrays of Molecules. *Adv. Mater.* **1998**, *10* (13), 1009−1013.
(44) Izhaky, D.; Addadi, L. Stereoselective Interactions of a Specialized Antibody with Cholesterol and Epicholesterol Monolayers. *Chem. −Eur. J.* **2000**, *6* (5), 869−874.
(45) Geva, M.; Izhaky, D.; Mickus, D. E.; Rychnovsky, S. D.; Addadi, L. Stereoselective Recognition of Monolayers of Cholesterol,Ent-Cholesterol, and Epicholesterol by an Antibody. *ChemBioChem* **2001**, *2* (4), 265−271.
(46) Wang, X.; Gan, H.; Sun, T.; Su, B.; Fuchs, H.; Vestweber, D.; Butz, S. Stereochemistry Triggered Differential Cell Behaviours on Chiral Polymer Surfaces. *Soft Matter* **2010**, *6* (16), 3851−3855.
(47) Zimmerman, E.; Geiger, B.; Addadi, L. Initial Stages of Cell-Matrix Adhesion Can Be Mediated and Modulated by Cell-Surface Hyaluronan. *Biophys. J.* **2002**, *82* (4), 1848−1857.
(48) Jiang, L.; Titmuss, S.; Cowley, A.; Klein, J. Direct Measurement of Forces between Cell-Coating Polymers and Chiral Crystal Surfaces: The Enantioselectivity of Hyaluronan. *Soft Matter* **2008**, *4* (7), 1521−1530.
(49) Baranes, K.; Moshe, H.; Alon, N.; Schwartz, S.; Shefi, O. Neuronal Growth on L - and D -Cysteine Self-Assembled Monolayers Reveals Neuronal Chiral Sensitivity. *ACS Chem. Neurosci.* **2014**, *5* (5), 370−376.
(50) Bonta, I. L.; De Vos, C. J.; Grijsen, H.; Hillen, F. C.; Noach, E. L.; Sim, A. W. 1-Hydroxy-3-Amino-Pyrrolidone-2 (HA-966): A New GABA-like Compound, with Potential Use in Extrapyramidal Diseases. *Br. J. Pharmacol.* **1971**, *43* (3), 514−535.
(51) Shepard, P. D.; Connelly, S. T.; Lehmann, H.; Grobaski, K. C. Effects of the Enantiomers of (±)-HA-966 on Dopamine Neurons: An Electrophysiological Study of a Chiral Molecule. *Eur. J. Pharmacol.* **1995**, *285* (1), 79−88.
(52) Macrae, C. F.; Sovago, I.; Cottrell, S. J.; Galek, P. T. A.; McCabe, P.; Pidcock, E.; Platings, M.; Shields, G. P.; Stevens, J. S.; Towler, M.; Wood, P. A. Mercury 4.0: From Visualization to Analysis, Design and Prediction. *J. Appl. Crystallogr.* **2020**, *53* (Pt 1), 226−235.
(53) *Apex3, [Computer Software]*; Bruker AXS Inc.: Madison, WI, USA, 2015.
(54) Sheldrick, G. M. *SHELXT* − Integrated Space-Group and Crystal-Structure Determination. *Acta Crystallogr., Sect. A: Found. Adv.* **2015**, *71* (1), 3−8.
(55) Sheldrick, G. M. Crystal Structure Refinement with *SHELXL*. *Acta Crystallogr., Sect. C: Struct. Chem.* **2015**, *71* (1), 3−8.
(56) Mehl, M. J.; Hicks, D.; Toher, C.; Levy, O.; Hanson, R. M.; Hart, G.; Curtarolo, S. The AFLOW Library of Crystallographic Prototypes: Part 1. *Comput. Mater. Sci.* **2017**, *136*, S1−S828.
(57) Subramanian, V.; Rowland, C. A.; Yap, G. P. A.; Martin, D. C. Morphology, Molecular Orientation, and Solid-State Characterization

https://doi.org/10.1021/acsomega.3c07719
ACS Omega 2024, 9, 13655−13665

of 2,3-Dihydrothieno[3,4- *b*][1,4]Dioxine-2-Carboxylic Acid (EDOTacid). *Cryst. Growth Des.* **2019**, *19* (11), 6184−6191.

https://doi.org/10.1021/acsomega.3c07719
ACS Omega 2024, 9, 13655−13665